Proceedings World Geothermal Congress 2020+1
Reykjavik, Iceland, April - October 2021

Uncertain Estimation of Clay Cap Boundaries using Magnetotelluric and MeB Data: Application to Wairākei Geothermal Field

Alberto Ardid[1], David Dempsey[1], Edward Bertrand[2], Fabian Sepulveda[3], Flora Solon[4], Pascal Tarits[4], Rosalind Archer[1]

[1]Engineering Science, University of Auckland, Auckland 1142, New Zealand

[2]GNS Science, 1 Fairway Drive, Avalon, Lower Hutt 5010, New Zealand

[3]Contact Energy Ltd, Wairakei Power Station, Te Aro Rd, Taupo 3352, New Zealand

[4]IUEM, Place Nicolas Copernic, F29840, Plouzané, France

aard708@aucklanduni.ac.nz

Keywords: Geothermal field, stochastic inversion, magnetotelluric, MeB

ABSTRACT

While the magnetotelluric (MT) method has been used in geothermal exploration for many years, the integrated evaluation of the effects of reservoir temperature, clay alteration, salinity and permeability on electrical resistivity have remained highly qualitative. In order to contribute to quantifying these effects, we develop an inversion methodology that integrates methylene blue (MeB) logs from wells with the electrical resistivity distribution from MT surveys. We use this method to infer, under uncertainty, clay cap boundaries in a geothermal field. Our methodology is based on a fast stochastic inversion of MT signals using Markov Chain Monte Carlo (MCMC) to fit a one-dimensional three-layer resistivity model beneath each MT station, laterally constrained by MeB data. The advantage of our approach is the explicit investigation and visualization of inversion uncertainty, yielding inferred depth intervals for clay cap boundaries. The methodology is tested on a profile of MT stations and MeB logs in wells located in the western area of the Wairākei geothermal field in the Taupō Volcanic Zone, New Zealand. Over the long-term, our goal is to improve our knowledge of uncertainty related to MT signals and its graphical representation to enhance our understanding of the relationship between resistivity and the clay cap.

1. INTRODUCTION

MT surveys have been largely used to image crustal (up to 10 km depth) and shallow (topmost 2 km depth) resistivity in geothermal areas (e.g. Gunderson et al., 2000; Ussher et al ., 2000; Caldwell et al., 2004; Heise et al., 2008; Bertrand et al. 2015), for hydrocarbon exploration (e.g. Firda et al., 2018) and tectonic studies (e.g. Stanley et al., 1990; Tietze et al., 2013). The advantages of MT in geothermal exploration relies on the substantial sensitivity of electrical resistivity (or its inverse, conductivity) to variations in swelling clay, temperature, salinity and permeability that in turn vary between rock type and formation. In addition, MT has a higher penetration depth compared to other electrical and EM geophysical methods, and deterministic inversion techniques have been developed to the point that 3D modelling is possible.

Deterministic inversion modelling of MT has been applied to the Taupō Volcanic Zone (TVZ), New Zealand's central North Island (e.g. Bertrand et al. 2012, 2013, 2015) to explore the resistivity structure up to a depth of 10 km, extending previous DC resistivity surveys of the near surface (Bibby, 1988). Major findings suggest several influences on the convective heat flow including magmatic intrusions, geological structures and migration of high-temperature saline fluids upwelling in fractures. Sepulveda et al. (2012) presented an integrated interpretation for Wairākei geothermal field (TVZ, NZ) of 1D and 3D MT inversions with drill-hole data and aeromagnetic data. With some exceptions, major results suggest a correlation between the base of shallow conductive bodies, the base of smectite clay zones, the 200°C isotherm, and the presence of deep conductors in some parts of the field.

Primarily, gradient-based deterministic inversions have been used to model MT data, and these have been successful in solving a wide range of problems with up to tens of millions of unknowns. This approach resolves resistivity gradients better than absolute resistivity values. With different starting models, sometimes the absolute resistivity values will increase/decrease, but the resistivity gradient, which 'maps' the resistivity structure, should be consistent. However, gradient-based deterministic inversions often tend to be dependent on the initial condition, suggesting that a local rather than a global solution has been achieved. In addition, more information about the uncertainty or non-uniqueness of the inversion would be valuable for decision-makers.

Geophysical stochastic inversion methods have proven a compelling alternative to deterministic approaches, e.g. Tarantola (2005), Chen et al. (2008). Their major limitation is due to their computational requirements that make their application non-viable for many parameters. Nevertheless, they can provide more detailed uncertainty information on parameter estimation, and the solutions tend to be less biased on the initial conditions. Some exciting examples of application in geothermal fields can be found in Kumar et al. (2010) where the role of 1D MT inversion is analyzed in the Darajat geothermal field (West Java, Indonesia), and in Chen et al. (2012) where the application of a 2D MT stochastic inversion is explored for the same Indonesian geothermal field.

In geothermal exploration, MT surveys are employed to identify the extent and thickness of the low permeable smectite clay cap that works as a cap rock in some systems. The presence of smectite clays could serve as a temperature indicator as it tends to form within a certain temperature range, 180-220°C (Morrison, 1997; Gunderson et al., 2000). Dempsey et al. (2016b) explored the use of 1D analytical solutions of heat and mass transfer to extrapolate temperatures to other parts of the reservoir by the correlation of MT inverted resistivity and temperature in a well. Results for a 2D synthetic reservoir model suggested a sensible capability to extrapolate temperature up to some kilometres from a well. An improvement to this extrapolation is presented in Ardid et al. (2018) by the

introduction of a 3-layer MT stochastic inversion that allows the uncertain estimation of top and bottom boundaries of clay cap and the uncertain extrapolation of isotherms away from the well. This is extended in Dempsey et al (2019) in two main aspects: the use of lithological information as a constraint for the MT inversion and the extrapolation of temperature from more than one well, still in a synthetic geothermal environment. Similar approaches to integrating reservoir and geophysical data are presented in Mellors et al. (2013, 2015).

In this study, we explore a real application of the MT inversion presented in Ardid et al. (2018) and extended in Dempsey et al. (2019), in the Wairākei geothermal field, located in the TVZ. We employed a set of data comprising an MT survey and MeB logs in wells from the geothermal field. For a NW-SE 2D profile (See Figure 1), we estimated with uncertainty the top and bottom boundaries of a shallow conductor revealed by the MT inversion that could be associated with the clay cap. We introduce the use of MeB data as a lithological constraint for the MT stochastic inversion and explore the limitations of the methodology.

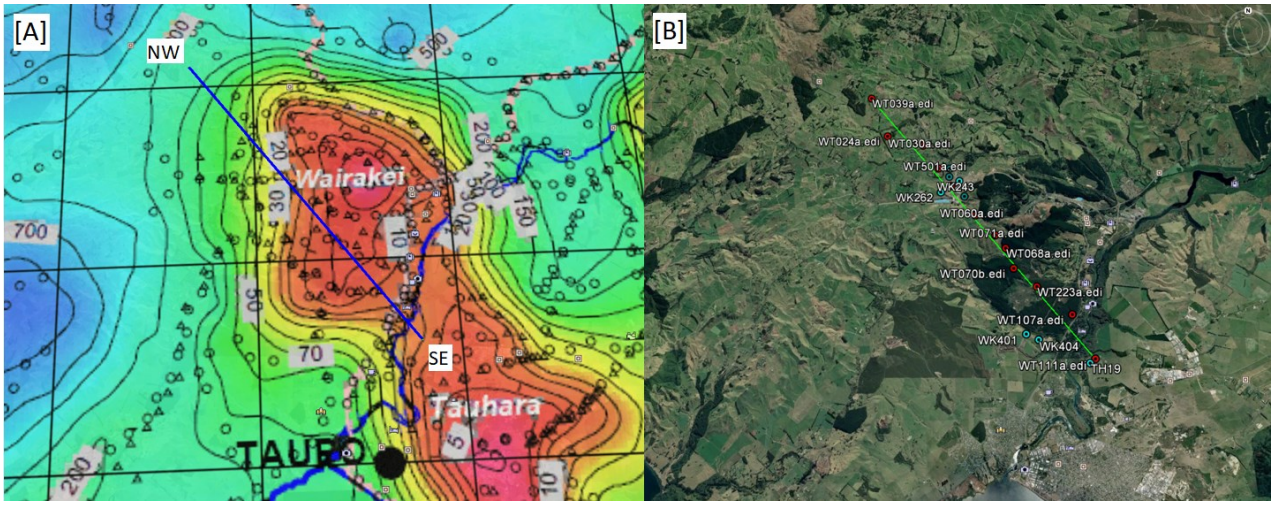

Figure 1: [A] shows the position of the 2D NW-SE modeled profile (blue line) superimposed on the resistivity map (~250 m depth) derived from previous DC studies (Risk, 1984). [B] shows the same profile (green line), the MT station (red dots) and wells (light blue) considered for the inversion superimposed on the topography.

2. FIELD AREA AND DATA SET

Our field area is the Wairākei-Tauhara geothermal field located within the TVZ in the North Island of New Zealand. The TVZ is a rifted continental arc around 300 × 60 km in dimension, situated at the southern extension of the Tonga-Kermadec subduction system (Wilson et al.,1995). The extension rate is ~ 2-8 mm/yr in the NW-SE direction. The TVZ formed in response to the westerly oblique subduction of the Pacific Plate beneath the Australian Plate along the Hikurangi Margin (Cole & Lewis, 1981). Comprehensive reviews of the geological structure of TVZ can be found in Cole et al. (1995), Rowland et al. (2010) and Seebeck et al. (2014).

Wairākei-Tauhara is located at the northeast of Lake Taupō in the central TVZ, and delineated by its DC resistivity boundary (Risk, 1984; Fig. 1). The field is thought to reflect the location of a primordial magmatic heat source within the crust. Wairākei-Tauhara is located in a deep and broad depression of the Greywacke basement filled mainly by low-density pyroclastic deposits and sediments. It presents complex lateral and vertical variation in lithological extent and thickness (Hunt et al., 2009). Stratigraphy has been reviewed by Rosenberg et al. (2009a) and updated by Bignall et al. (2010a).

Hydrothermal alteration at Wairākei-Tauhara increases in rank and intensity with depth. For the superficial units, the alteration has been found to be argyllic (smectite and illite) being moderate in Oruanui and high in Huka Falls Formation. For the Waiora formation the alteration has been found to be propylitic type (chloride, quartz and epidote). The chemical evolution and degree of alteration are not homogenous for the whole field, being more severe in western Wairākei. The Wairākei ignimbrite also presents a degree of alteration, which is indicative of the age of the field, and suggests that it has been active for at least 500 kyr (Grindley, 1965).

In this study, we jointly model two sets of data localized in one profile (See Figure 1), in order to obtain the distribution of resistivity in the subsurface. The data set includes impedance data from 13 MT stations and MeB (Methylene Blue) logs from 10 wells. The MT data is a subset of an extended survey that the field operator undertook in early 2010. The profile crosses inner and outer sections of the field, which is ideal to explore how the methodology captures the presence or absence of the clay cap and the uncertainty related to the estimation (Fig. 1).

3. METHODOLOGY

The formulation for field application of the stochastic 1D MT inversion for each station is presented below. The principal innovation is the introduction of lithological information from multiple wells as a constraint on the inversion. MeB data, an indicator of conductive clay content (Gunderson et al., 2000), is used to estimate the vertical extent of the primary conductor in the MT inversion. This constraint is imposed through the inclusion of priors on the boundaries of a parameterized 3-layer resistivity model in the MT inversion. The prior is calculated for each MT station using the nearest wells available. Then, the apparent resistivity and phase of

the off-diagonal impedance tensor terms, Zxy and Zyx, are jointly inverted with the same weights, as a 1D representation of the three-dimensional impedance tensor.

3.1 MT inversion: Stochastic formulation

Data from MT stations is inverted using MCMC to calibrate the parameters of a 3-layer resistivity model in each station. The parameters are five: the thickness of the top two layers, and resistivities for the two layers and a bottom half-space. The middle layer is assumed to be an electrical conductor, representing the depth and thickness of the clay cap at that location. It is assumed that their values are independent in the vertical direction and dependent in the horizontal direction, where the dependency is model as a Gaussian prior using MeB content from the nearest wells.

The joint posterior probability distribution that define the Bayesian model of the unknown parameters at each MT station is:

$$f(\rho, z|\hat{\rho}) \propto f(\hat{\rho}|\rho, z) \prod_{i=1}^{N_{layers}} f(\rho_i) \prod_{j=1}^{N_{boundaries}} f(z_j) \quad (1)$$

Where $\hat{\rho}$ represents the MT data across all frequencies, z represents the unknown depths of layer boundaries, and ρ the unknown layer resistivities. The first function of the right hand side corresponds to the likelihood function that relates the MT data with the resistivity model. The second and third functions correspond to prior distributions for resistivity and boundary depths that we use to incorporate a priori information of the parameters revealed by lithological information from nearest wells.

3.1.1 Prior probability distribution of resistivity

To constrain the MT inversion in each station, we construct prior distributions for the parameters based on a priori information. Regarding resistivities for the 3-layer model, based on conceptual resistivity models for geothermal reservoirs (Oskooi et al., 2005), we assume that for the shallow zone a lower resistivity anomaly is related to the presence of a clay cap. Conductive smectite clays usually present with resistivities lower than 5 Ohm m.

We impose this information as a uniform distribution that models the range for the resistivity value of the second layer. For the upper and lower layers, we do not impose prior information on their resistivity values, letting them vary freely. Then, the uniform prior distribution for the resistivity of the second layer is given by:

$$f(\rho_2) = Ind[\rho \epsilon (0,5)] \quad (2)$$

Where $Ind[]$ represents the indicator function having the value one if the condition inside the bracket is satisfied and zero otherwise.

3.1.2 Prior probability distribution of depth and MeB data

MeB content is an indirect indicator of contrast in electrical resistivity as it measures the presence of smectite, which is a highly conductive clay. We use this information to construct Gaussian priors on the upper and lower boundary of the conductive layer.

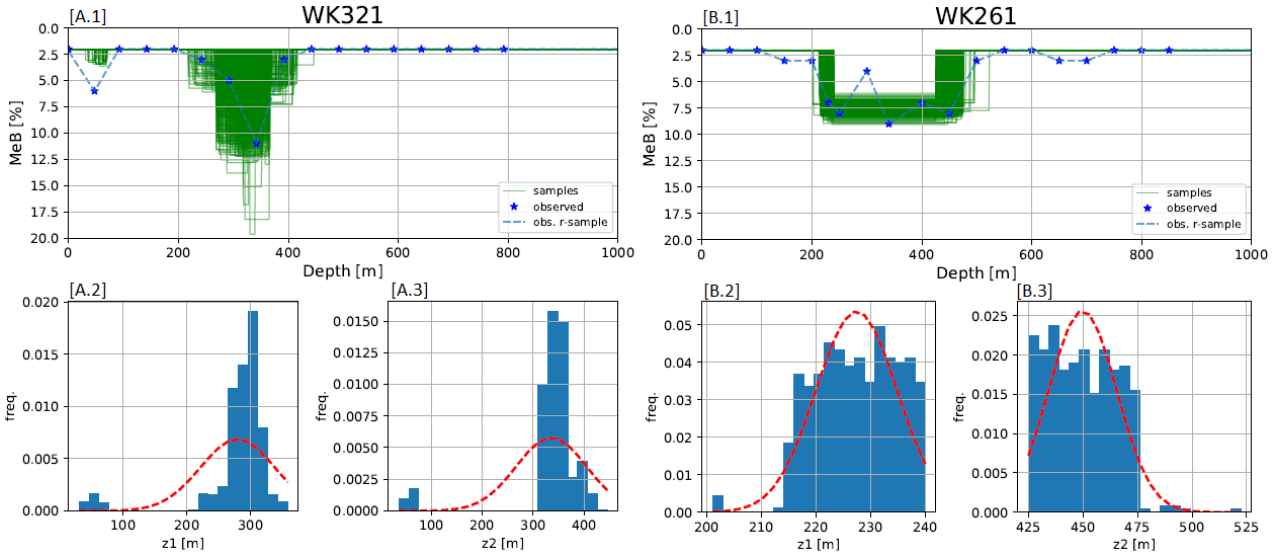

Figure 2: MeB MCMC inversion results for wells WK321 [A] and WK261 [B], obtained by fitting a square function to the MeB profile. [A.1] and [B.1] shows MeB samples (blue '*') and multiple model fits from the posterior function (green lines). [A-B.2] and [A-B.3] show the distribution of the square function corners generated from the samples, quantifying the depths of occurrence for the clay cap boundaries at the well, and the uncertainty related to it. A.2 and B.2 refers to the top boundary (z1) of the clay cap for the wells WK321 and WK261; A.3 and B.3 refers to the bottom boundary (z2) of the clay cap for the wells WK321 and WK261.

MeB logs measure the percentage of clay sampled at different depths. Figure 2 shows an example of a MeB profile, where values over 2% can reliably be considered as clays. Although there is no direct relationship between the clay content and resistivity, the relative abundance of clay is nevertheless a useful indicator of the boundaries of the conductor in the vicinity of that well.

To obtain distributions on boundaries of the clay cap at the well location, we invert the MeB profiles using MCMC and fitting a square function. This simple model is sufficient to capture the sudden appearance and disappearance of clay in the log. In Figure 2, samples from the posterior function show that the fitting routine generates square functions whose corners concentrate at certain depths. Histogram plots of these boundaries indicate that at WK243 the top of the conductor is between 100 and 150 m depth, and the bottom is 250 and 350 m depth.

Once priors for the clay cap boundaries have been obtained, these need to be interpolated to the MT station where an inversion is to be performed (these will not generally be coincident with the wells where MeB is logged). For this, we use a distance weighted average of the nearest wells (up to four). Figure 3 demonstrates this for a station located at 'j' between two wells at 'i' and 'i+1'. Once the distribution parameters are calculated for each MT station position, the prior probability distribution for depth is given by:

$$f(z_j) \propto \lambda * exp(-|z_j - z_j^w|^2 / \sigma_j^w) \quad (3)$$

Where j corresponds to the boundary layer, z_j is the depth model to the boundary layer j, z_j^w and σ_j^w the weighted average depth and standard deviation calculated from nearest wells. λ corresponds to a weight parameter equal to $exp(-2 * d)$, with d the distance to the closest well considered in the prior.

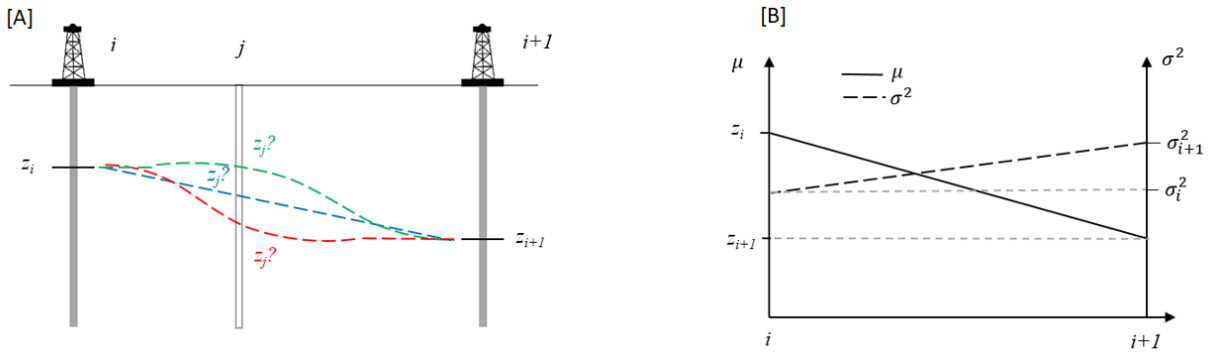

Figure 3: Uncertain layer position at j between known depths at i and i+1. [A] Blue, red and green dashed lines show possible interface positions. [B] Mean (solid) and variance (dashed) of prior distribution for inversion at j between i and i+1 (modified from Dempsey et al., 2019).

3.1.3 Likelihood probability function and MT data

The likelihood function for MT data is given by the misfit between the data and the corresponding simulation results assuming normally distributed errors. The function plays a key role as it is the link between the unknown parameters and the MT data. Although in practice total error (residual of the misfit) is combines both measurement error and forward modeling errors, here we have had to assume that the error is attributable to measurement deficiency only. This simplification is valid providing the model errors are significantly smaller than the measurement errors, which may not always be the case when using a simplified 3-layer model.

The likelihood function for each MT station is given by:

$$f(\rho, z) \propto \prod_{p=1}^{N_{periods}} exp(-|z_{obs} - z_{mod}|_p^2 / 2\sigma^2) \quad (4)$$

Where z^{obs} and z^{mod} are the observed and simulated data, for period, p. σ^2 is the measurement error. The data correspond to the apparent resistivity and phase of the off-diagonal impedance elements

Figure 4 shows an example of the data that are being fitted: the apparent resistivity and phase for the off-diagonal impedance tensor terms, Zxy and Zyx. The fitting samples are synthetic observations generated from different models (a combination of parameters for a 3-layer resistivity model) extracted from the posterior distribution of model parameters. The misfit is calculated as the difference between the observation and sample for each period.

The data (Figure 4) shows a one-dimensional behavior up to the period ~ 1 s, correctly approximated by the model. Depths reached by this period (~ 3-5 km depth) are enough to characterize the anomaly of low resistivity generated by the clay cap, validating the 1D approach for shallow depths in the profile. For higher periods, the transition to a two-dimensional resistivity distribution is observed, being the response of our model a sort of average between Zxy and Zyx components of the impedance tensor.

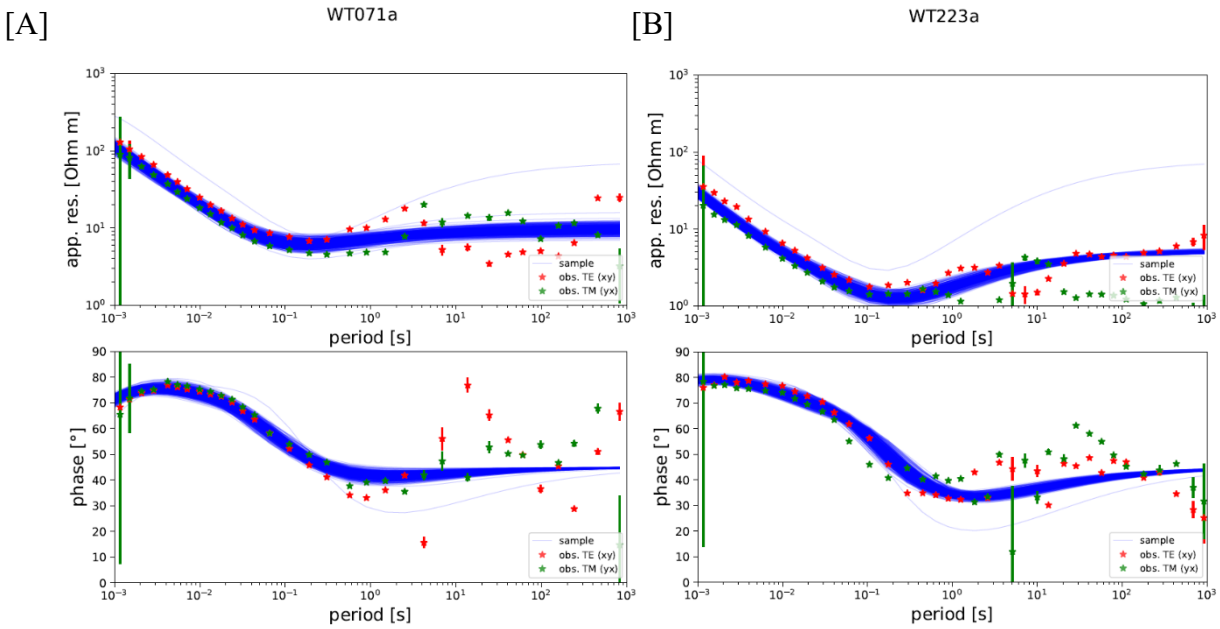

Figure 4: Apparent resistivity and phase for stations WT071a [A] and WT223a [B] shown as '*' for off-diagonal impedance tensor terms, XY and YX . Fitting samples derived from posterior distribution result from MCMC MT inversion are shown in blue lines.

4. RESULT AND DISCUSSION

The stochastic inversion described in the previous section has been performed for the MT stations shown in the profile in Figure 1. From this, we obtain an uncertain estimate along the profile of the bottom and top boundaries distribution for the shallow conductor.

4.1 Uncertain top and bottom boundaries of clay cap

We are interested in visualizing the uncertainty associated with the top and bottom boundaries of the clay cap. Therefore, for each of these boundaries, we plot shaded envelopes at each station location covering the 5-95% occurrence probability for that parameter. We also plot the distribution of clays obtained by inverting the MeB data from nearby wells.

Figure 5 shows the modeled profile introduced in Figure 1, where uncertain distributions for the inferred top and bottom boundaries of the clay cap are plotted. The inversion recovers a regular thickness for the clay cap, averaging about 100 [m], consistent with most of the results from MeB inversion. For the top boundary, less uncertainty is observed compared to the bottom one. This is expected for an MT inversion where a conductive layer attenuates signal strength. Uncertainty associated with the depth of the top boundary is about ~50 [m] whereas for the bottom boundary it is about ~150 [m].

In the NW section of the profile, the second layer thins to less than the resolution of the MT method, indicating that, for this area, the middle conductive layer is not necessary to fit the MT data (but it is nevertheless forced to by our imposed model). Thus, this end of the profile is interpreted as the absence of a clay cap in the section beneath stations WT039a and WT024a. This is consistent with Figure 1 where these stations are identified to be outside the main reservoir area, defined by the DC resistivity boundary (Risk et al., 1984), and where no clay cap is expected.

Below station WT030a, a thicker section is observed, that could be related to a thick clay cap or due to a deep conductor that could be influencing the shallow high conductive response. A deep conductor has been found in this area as indicated by deeper 3D MT inversions (Sepulveda et al., 2012), related to relict alteration.

Around station WT502a, a coherent correlation is observed between the uncertain boundaries obtained from the MT inversion and the MeB inversion results, clearer for the top boundary and less for the bottom where the uncertainty in the MeB results are higher. Between stations WT223a and WT107a, the correlation is less clear since the two nearest wells (WK401-04) are not consistent in their clay content. For the station WK111a, the correlation with well TH19 is consistent.

The profile in Figure 5 is equivalent to the resistivity section WRKNW5 in Sepulveda et al., 2012 (Appendix 2, based on 3D MT models), where resistivity distribution is integrated with interpreted reservoir temperatures and stratigraphy. Regarding resistivity distribution, a good correlation for the low resistivity anomaly between section WRKNW5 and Figure 5 is observed, where the extension of the anomaly to the SE seems to be clearer from our results. Depths seems to be well correlated too, where our methodology more useful in estimating boundaries for this conductive structure. As in section WRKNW5, the bottom of the conductor in Figure 5 looks correlated with isotherm 180-200°C for the mid-NW section around WT502a, but from WT060a to the SE it appears to be following the top of rhyolite Karapiti 2A rather than the isotherm. Sepulveda et al., 2012 suggest that the bottom boundary of the observed low resistivity anomaly could be indicating the top boundary of the rhyolite (high-permeable boundaries and low-permeable cores), reflecting permeability distribution rather than temperature distribution.

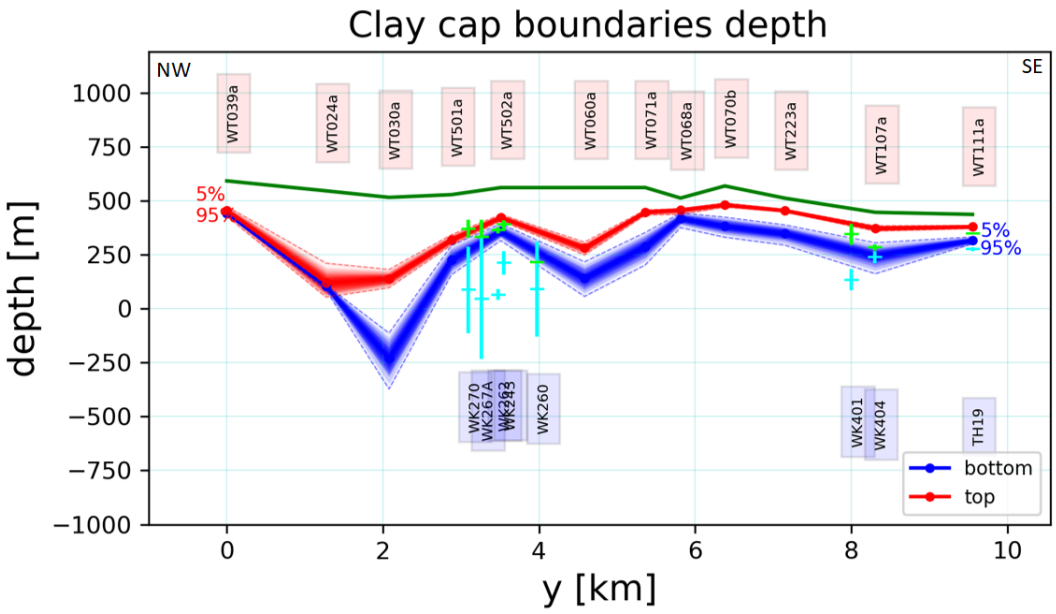

Figure 5: Uncertain depth distributions of top and bottom boundaries of the high conductive second layer, representative of the clay cap, for the profile in Figure 1. Shaded envelopes are plotted covering between 5%-95% of occurrence probability. Distribution of clay cap boundaries obtained by inverting the MeB data are plotted (green cruxes for top boundary and light blue cruxes for the bottom boundary). Name of MT stations inverted at the top (red boxes). Name of MeB wells at the bottom (blue boxes). The green line shows the topography.

5. SUMMARY

We have developed an integrated methodology that allows for the joint modeling of MT data with MeB logs from wells. First, we developed a stochastic inversion of MT constrained by MeB logs from wells. Then, we infer within uncertainty the clay cap boundaries in a geothermal field. In this study, we have presented an application of the method to the Wairākei-Tauhara geothermal field in New Zealand.

The methodology (Section 3.1) is formulated as a fast stochastic inversion of MT constrained by MeB logs from nearby wells. Results have shown (Figures 2, 4 and 5) that modeling MeB data (an indirect indicator of resistivity) is useful for inverting MT data providing the inversion model explicitly builds in a middle conductive layer. Furthermore, the MeB inversion proposed, and the integration of their results to the stochastic formulation, is reasonably computationally efficient to implement.

For the uncertain estimation of the clay cap boundaries (Figure 5), the results are consistent with the resistivity boundary for Wairākei, capturing the absence of the clay cap in the outfield section of the profile. Results are also consistent with the boundaries derived from the MeB inversion and a coherent structure for the clay cap is obtained.

The next steps for our methodology are to develop validation strategies for clay cap boundary estimates, by profiling for different parts of the field and comparing the MT inversion estimates with standard inversion software. In addition, we are extending the methodology for an uncertain extrapolation of isotherms away from wells in the Wairākei geothermal fields, following Ardid et al. (2018) and Dempsey et al. (2019).

ACKNOWLEDGEMENTS

Contact Energy Ltd. is thanked for data support and permission to publish data. The authors also thank funding from the Ministry for Business, Innovation and Employment from New Zealand through the Empowering Geothermal and Dumont d'Urville grants and the Faculty of Engineering at the University of Auckland.

REFERENCES

Ardid, A., Dempsey, D., Bertrand, T., and Archer, R.: Uncertain Estimation of Subsurface Temperature Away from the Borehole Using Magnetotelluric Inversions, Proceedings, 40th New Zealand Geothermal Workshop, Taupō, New Zealand (2018).

Bertrand, E.A., Caldwell, T.G., Hill, G.J., Wallin, E.L., Bennie, S.L., Cozens, N., Onacha, S.A., Ryan, G.A., Walter, C., Zaino, A., Wameyo, P.: Magnetotelluric imaging of upper-crustal convection plumes beneath the Taupō Volcanic Zone, New Zealand. Geophys. Res. Lett. 39. http://dx.doi.org/10.1029/2011GL050177 (2012).

Bertrand, E.A., Caldwell, T.G., Hill, G.J., Bennie, S.L., Soengkono, S.: Magnetotelluric imaging of the Ohaaki geothermal system, New Zealand: implications for locating basement permeability. J. Volcanol. Geotherm. Res. 268, 36–45. http://dx.doi.org/10.1016/j.volgeores.2013.10.010. (2013).

Bertrand E.A., Caldwell T.G., Bannister S., Soengkono S., Bennie S.L., Hill G.J., Heise W.: Using array MT data to image the crustal resistivity structure of the southeastern Taupō Volcanic Zone, New Zealand, Journal of Volcanology and Geothermal Research, Volume 305, 2015, Pages 63-75, ISSN 0377-0273, https://doi.org/10.1016/j.jvolgeores.2015.09.020. 14 (2015).

Bibby, H.M., Electrical resistivity mapping in the central volcanic region of New Zealand. N. Z. J. Geol. Geophys. 31, 259–274. (1988).

Bignall G., Browne P.R.L., Kyle P.R.: Geochemical characterisation of hydrothermally altered ignimbrites in active geothermal fields from the central Taupō Volcanic Zone, New Zealand. Journal of Volcanology and Geothermal Research 73: 79–97. (1996).

Caldwell, T.G., Bibby, H.M., Brown, C.: The magnetotelluric phase tensor. Geophys. J. Int. 158, 457–469 (2004).

Chen, J., Hoversten, G, Key, K., Nordquist, G.: Stochastic inversion of 2D magnetotelluric data using sharp boundary parameterization. SEG Technical Program Expanded Abstracts. 29. 10.1190/1.3513857. (2010).

Chen, J., A. Kemna, and S. Hubbard.: A comparison between Gauss-Newton and Markov chain Monte Carlo based methods for inverting spectral induced polarization data for Cole-Cole parameters: Geophysics, 73, no. 6, F247–F259, doi: 10.1190/1.2976115. (2008)

Cole J.W., Lewis K.: Evolution of the Taupō-Hikurangi subduction system. Tectonophysics 72:1–21. (1981).

Cole J.W., Darby D.J., Stern T.A.: Taupō Volcanic Zone and Central Volcanic Region: Back arc structures of North Island, New Zealand. In: Taylor B. ed. Backarc Bains: Tectonics and Magmatism. Plenum Publishing, New York. Springer. Pp. 1–28. (1995).

Dempsey, D., O'Sullivan, J., and Pearson, S.: Joint Inversion of Temperatures in a Synthetic Geothermal Field using MT, Clay Alteration Models, and Geothermal Reservoir Simulation, Proceedings, 38th New Zealand Geothermal Workshop, Rotorua, New Zealand (2016b).

Dempsey D., Riffault, J., Ardid, A., Bertrand T., Archer R.: Integrating Magnetotelluric and Microseismic Data with Geothermal Reservoir Models, Proceedings, 44th Workshop on Geothermal Reservoir Engineering, Stanford University, Stanford, CA (2019).

Firda I., S, Permadi N., Suparno A., Supriyanto, Suwardi, B.: Hydrocarbon Reservoir Identification in Volcanic Zone by using Magnetotelluric and Geochemistry Information. IOP Conference Series: Earth and Environmental Science. 132. 012018. 10.1088/1755-1315/132/1/012018. (2018).

Gunderson, R., Cumming, W., Astra, D., Harvey, C.: Analysis of Smectite Clays in Geothermal Drill Cuttings by the Methylene Blue Method: For Well Site Geothermometry and Resistivity Sounding Correlation, Proceedings World Geothermal Congress 2000 in Kyushu - Tohoku, Japan, May 28 - June 10. (2000)

Heise, W., Caldwell, T.G., Bibby, H.M., Bannister, S.C.: Three-dimensional modelling of magnetotelluric data from the Rotokawa geothermal field, Taupō Volcanic Zone, New Zealand. Geophys. J. Int. 173, 740–750. http://dx.doi.org/10.111/j.1365-246X.2008.03737.x. (2008).

Hunt T.M., Bromley C.J., Risk G.F., Sherburn S., Soengkono S.: Geophysical investigations of the Wairākei Field. Geothermics 38: 85–97. (2009).

Kumar, D., Hoversten, G.M., Nordquist, G., Cumming, W.,: Role of 1D MT inversionin a 3D geothermal field. 80th Annual International Meeting, SEG, Expanded Abstracts 1107–1111. (2010).

Rosenberg M.D., Bignall G., Rae A.J.:The geological framework of the Wairākei Tauhara Geothermal System, New Zealand. Geothermics 38: 72–84. (2009a)

Rowland J.V., Wilson C.J.N., Gravley D.M. Spatial and temporal variations in magma-assisted rifting, Taupō Volcanic Zone, New Zealand. Journal of Volcanology and Geothermal Research 190:89–108. (2010) .

Mellors, R. J., Ramirez, A., Tompson, A., Chen, M., Yang, X., Dyer, K., Wagoner, J., Foxall, W., and Trainor-Guitton, W.: Stochastic Joint Inversion of a Geothermal Prospect, Proceedings, 38th Workshop on Geothermal Reservoir Engineering, Stanford University, Stanford, CA (2013)

Mellors, R. J., Tompson, A., Yang, X., Chen, M., Ramirez, A., and Wagoner, J.: Stochastic Joint Inversion Modeling Algorithm of Geothermal Prospects, Proceedings, 40th Workshop on Geothermal Reservoir Engineering, Stanford University, Stanford, CA (2015).

Morrison, K.: Important hydrothermal minerals and their significance, Geothermal and Mineral Service Div., Kingston Morrison Ltd (1997).

Seebeck H., Nicol A., Villamor P., Ristau J., Pettinga J.: Structure and kinematics of the Taupō Rift, New Zealand. Tectonics 1178–1199. (2014).

Sepulveda, F., T. Glynn-Morris, W. Mannington, J. Charroy, S. Soengkono, G. Ussher: "Integrated approach to interpretation of magnetotelluric study at Wairākei, New Zealand." Proceedings of the 36th Workshop on Geothermal Reservoir Engineering, 30 Jan. – 1 Feb., Stanford University, Stanford, California (2012).

Stanley,W.D., Mooney,W.D., Fuis, G.S.: Deep crustal structure of the Cascade range and surrounding regions from seismic refraction and magnetotelluric data. J. Geophys. Res. 95, 19419–19438 (1990).

Oskooi B., Pedersen L. B., Smirnov M., Árnason K., Eysteinsson H., Manzella A.:The deep geothermal structure of the Mid-Atlantic Ridge deduced from MT data in SW Iceland, Physics of the Earth and Planetary Interiors, Volume 150, Issues 1–3, Pages 183-195, ISSN 0031-9201, https://doi.org/10.1016/j.pepi.2004.08.027. (2005).

Tarantola, A.: Inverse problem theory and methods for model parameter estimation: The Society for Industrial and Applied Mathematics (SIAM) (2005).

Tietze, K., Ritter, O.: Three-dimensional magnetotelluric inversion in practice — the electrical conductivity structure of the San Andreas Fault in central California. Geophys. J. Int. http://dx.doi.org/10.1093/gji/ggt234. (2013).

Usher, G., Harvey, C., Johnstone, R., Anderson, E.: The resistivity structure of high-temperature geothermal systems in Iceland. Proceedings World Geothermal Congress 2000 in Kyushu - Tohoku, Japan, May 28 - June 10. (2000)

Wilson C.J.N., Houghton B.F., McWilliams M.O., Lanphere M.A., Weaver S.D., Briggs R.M.: Volcanic and structural evolution of Taupō Volcanic Zone, New Zealand: a review. Journal of Volcanology and Geothermal Research 68: 1–28. (1995).